Magnetic field dipolarization in the deep inner magnetosphere and its role in development of O

AUTHOR(S):

Nosé, M.; Koshiishi, H.; Matsumoto, H.; C:son Brandt, P.; Keika, K.; Koga, K.; Goka, T.; Obara, T.

JOURNAL OF GEOPHYSICAL RESEARCH, VOL. 115, A—, doi:10.1029/2010JA015321, 2010

Magnetic field dipolarization in the deep inner magnetosphere and its role in development of O^+-rich ring current

Nosé, M.,[1] H. Koshiishi,[2] H. Matsumoto,[2] P. C:son Brandt,[3] K. Keika,[4] K. Koga,[2] T. Goka,[2] and T. Obara[2]

Abstract.

We studied magnetic fiel dipolarization and associated ion acceleration in the deep inner magnetosphere, using magnetic fiel data obtained by the magnetometer (MAM) onboard the Mission Demonstration Satellite -1 (MDS-1) satellite and the energetic neutral atom (ENA) flu data obtained by the high-energy neutral atom (HENA) imager onboard the Imager for Magnetopause-to-Aurora Global Exploration (IMAGE) satellite. Since the MDS-1 satellite has a geosynchronous transfer orbit, we could survey magnetic fiel variations at L=3.0-6.5. We analyzed data in the period from February to July in 2002. We found that (1) dipolarization can be detected over a wide range of L (i.e., L=3.5-6.5, which is far inside the geosynchronous altitude); (2) when the MDS-1 satellite was located close to auroral breakup longitude, the occurrence probability of dipolarization was about 50% just inside the geosynchronous altitude and about 16% at L=3.5-5.0, suggesting that dipolarization in the deep inner magnetosphere is not unusual; (3) magnetic storms were developing whenever dipolarization was found at L=3.5-5.0; (4) dipolarization was accompanied by magnetic fiel fluctuation having a characteristic timescale of 3-5 sec, which is comparable to the local gyroperiod of O^+ ions; and (5) after dipolarization, the oxygen ENA flu in the nightside ring current region was predominantly enhanced by a factor of 2-5 and stayed at an enhanced level for more than 1 hour, while clear enhancement was scarcely seen in the hydrogen ENA flux From these results, we conjectured a scenario for generation of O^+-rich ring current, in which preexisting thermal O^+ ions in the outer plasmasphere (i.e., an oxygen torus known from satellite observations) experience local and nonadiabatic acceleration by magnetic fiel fluctuation that accompany dipolarization in the deep inner magnetosphere (L=3.5-5.0).

1. Introduction

Magnetic fiel dipolarization (reconfiguratio from a taillike magnetic fiel to a dipolelike magnetic field is a distinct phenomenon observed in the magnetosphere at substorm onset. According to previous studies, magnetic fiel dipolarization can be mostly seen at the geosynchronous altitude or farther down the tail (i.e., radial distance (r) of $\geq$6.6 R_E).

One of the oldest papers reporting magnetic fiel dipolarization at the geosynchronous altitude (r=6.6 R_E) is a study by *Cummings et al.* [1968] who used the ATS-1 satellite. Magnetic fiel dipolarization in the near-tail region (r=9-13 R_E) was firs reported by *Heppner et al.* [1967] with the OGO-A satellite (see section 10 in their paper), which was followed by *Sugiura et al.* [1968] with a vector magnetic fiel measurement by the OGO-3 satellite. A review of geomagnetic tail fiel observation during substorms in the early space age is given by *McPherron et al.* [1973], who themselves presented dipolarization at r~8-11 R_E, using data from the OGO-5 satellite. Multisatellite observations made it possible to investigate propagation signatures of dipolarization. *Nagai* [1982] statistically studied magnetic fiel dipolarization by using two geosynchronous satellites (GOES-2 and -3) and found that it starts in a localized area and then develops longitudinally in both the westward and eastward directions. Magnetic fiel reconfiguration also propagates tailward from the geosynchronous altitude to X=−20 R_E or farther [*Lopez and Lui*, 1990; *Jacquey et al.*, 1991; *Ohtani et al.*, 1992a]. In some events, the dipolarization front expands even earthward from r~8.8 R_E to r~6.6 R_E [*Ohtani*, 1998]. As shown above, many observations of dipolarization have been done at $r\geq$6.6 R_E since the late 1960s, and countless papers have been published. Recent observations of dipolarization and related issues are summarized by *Lui* [2001] and *Angelopoulos* [2008].

On the other hand, a limited number of previous studies have reported magnetic fiel dipolarization inside the geosynchronous orbit. A statistical study of the occurrence probability of dipolarization was performed with the AMPTE/CCE satellite by *Lopez et al.* [1988]. They found that dipolarization can scarcely be seen inside the geosynchronous orbit and the innermost boundary is at r=6.4 R_E. The AMPTE/CCE satellite was operated during the solar minimum (1984-1987); however, the CRRES satellite made an observation during the solar maximum (1991) and found some dipolarization events at $r\leq$6.4 R_E [*Maynard et al.*, 1996; *Sergeev et al.*, 1998; *Fu et al.*, 2002]. *Maynard et al.* [1996] examined 8 events occuring at L=5.2-6.4 from January to March of 1991, one of which was also investigated in detail by *Sergeev et al.* [1998]. *Fu et al.* [2002] presented some dipolarization events detected at L=5.5-6.5 in March and May of 1991. Recently, *Ohtani et al.* [2007] investigated a magnetic fiel dipolarization observed at r=4.6 R_E by the Cluster satellites on 18 April 2002; the satellites were off the geomagnetic equator during the event, and thus L-values of the satellites are nearly the same as that of geosynchronous satellites (see their Figure 2b). Thus, to our knowledge, magnetic fiel dipolarization inside the geosynchronous orbit has been demonstrated for

[1]Data Analysis Center for Geomagnetism and Space Magnetism, Graduate School of Science, Kyoto University, Kyoto, Japan.
[2]Aerospace Research and Development Directorate, Japan Aerospace Exploration Agency, Tsukuba, Ibaraki, Japan.
[3]Applied Physics Laboratory, Johns Hopkins University, Laurel, Maryland, USA.
[4]Center for Solar-Terrestrial Research, New Jersey Institute of Technology, Newark, New Jersey, USA.

only about 10 events so far, and they were found down to a depth of L=5.2.

In this study, therefore, we pose the following 4 target questions to unveil detailed characteristics of magnetic f eld dipolarization in the deep inner magnetosphere (i.e., $r<6.6\ R_E$): (1) how deep can dipolarization be detected?; (2) how frequently can dipolarization be observed in the deep inner magnetosphere?; (3) does dipolarization in the deep inner magnetosphere show similar signatures to that at $r\geq 6.6\ R_E$?; and (4) does dipolarization in the deep inner magnetosphere contribute to ion acceleration and ring current formation? We tackle these questions using magnetic fiel data from the Mission Demonstration Satellite -1 (MDS-1) satellite and energetic neutral atom (ENA) data from the Imager for Magnetopause-to-Aurora Global Exploration (IMAGE) satellite.

This paper is organized as follows. In section 2, we describe the instrumentation and data set used in this study. In section 3, we analyze the magnetic fiel data from the MDS-1 satellite. Three typical examples of dipolarization in the deep inner magnetosphere will be demonstrated with results of their spectral analysis. Statistical analysis of dipolarization inside the geosynchronous altitude is also performed. Section 4 presents ENA data from the IMAGE satellite when the three dipolarization events occurred. In section 5, we answer the above 4 target questions and propose a new scenario for O^+-rich ring current generation. Section 6 summarizes the paper.

2. Instrumentation and Data Set

2.1. MDS-1 Satellite

The MDS-1 satellite was launched in February 2002 into a geosynchronous transfer orbit (GTO) having an apogee of 6.6 R_E, a perigee of 500 km altitude, an orbital period of about 10.5 hr, and an orbital inclination of 28.5°. The MDS-1 satellite carried a triaxial flux ate magnetometer (MAM), which was mounted at the end of a 3-m deployable mast to prevent electromagnetic disturbances from reaching the satellite body. MAM records data with a sampling rate of 8 Hz and is operated with three observation modes; the dynamic range and resolution of each mode are ±256 nT and 8 pT (mode 1), ±1024 nT and 31 pT (mode 2), and ±65536 nT and 2 nT (mode 3). The MAM data suffered from a satellite spin with a period of ∼11.5 sec, and its effect could not be removed completely by on-ground data processing, resulting in continuous sinusoidal oscillation. Therefore, we fitte a sine function having a period of ∼11.5 sec to the MAM data, and eliminated the sinusoidal oscillation as much as possible by subtracting the fitte sine function. A more detailed description of the MDS-1 satellite and the MAM instrument is found in *Koshiishi et al.* [2004].

The data period used here are from 11 February 2002 to 31 July 2002. Figure 1 shows the MDS-1 orbits on February 11, 1st day of every month from March to July, and July 31 in 2002 in the X-Y plane in solar magnetospheric (SM) coordinates. MDS-1 fl w mostly on the nightside during this period. The MDS-1/MAM data are used to identify magnetic fiel dipolarization in the deep inner magnetosphere.

2.2. IMAGE Satellite

The IMAGE satellite is a polar orbiting satellite with a perigee of 1000 km altitude, an apogee of 8.2 R_E, and an orbital period of 14.2 hr [*Burch*, 2000]. The satellite spins at a rate of ∼0.5 revolutions per minute and its spin vector is antiparallel to the orbital angular momentum vector. The high energetic neutral atom (HENA) imager on board the IMAGE satellite is designed to detect neutral hydrogen atoms in the energy range of 10-500 keV [*Mitchell et al.*, 2000]. The HENA imager has a fiel of view of ±60° against a satellite spin plane that is divided into 20 polar sectors for lower-energy hydrogen (<60 keV) and 40 polar sectors for higher-energy hydrogen (>60 keV). As the satellite spins, the imager sweeps out 360° in the azimuthal direction, which is divided into 60 azimuthal sectors for lower-energy hydrogen (<60 keV) and 120 azimuthal sectors for higher-energy hydrogen (>60 keV). This results in one 2-D complete image of lower-energy (higher-energy) hydrogen flu covering an area of 120°(polar)×360°(azimuth) with a 6°×6° (3°×3°) angular resolution every 2 min.

The energy band is divided into 6 steps for lower-energy hydrogen and 4 steps for higher-energy hydrogen. The fligh software was modifie in August 2001, and since then HENA has been able to separate oxygen emissions from hydrogen emissions [*Mitchell et al.*, 2003]. Oxygen is obtained in the 29-264 keV energy range divided into eight steps with the same temporal and spatial resolution as lower-energy hydrogen (i.e., 2 min and 6°×6°). We used the IMAGE/HENA data to examine ion acceleration and ring current formation associated with dipolarization in the deep inner magnetosphere.

3. Analysis of MDS-1/MAM Data

3.1. Event Selection

We selected dipolarization events occuring in the deep inner magnetosphere from the MDS-1/MAM data. First, we listed candidate events that satisfy the following three criteria: (1) MDS-1 was located at L=3.0-6.5, that is, sufficientl deep inside the geosynchronous orbit; (2) a well-developed auroral substorm was observed by the Far Ultra-Violet (FUV) imager on the IMAGE satellite; and (3) the separation in magnetic local time (MLT) between MDS-1 and auroral onset locations is less than or equal to 2.5 hr (i.e., $|\Delta\text{MLT}|\leq 2.5$ hr). In criterion 2, we used the onset list provided by *Frey et al.* [2004]. These criteria yielded 68 candidate events. Second, we created magnetic fiel variation data by subtracting the 10th generation International Geomagnetic Reference Field (IGRF) model fiel from the observed magnetic fields The variation data is represented as ΔV, ΔD, and ΔH in VDH coordinates, where H is antiparallel to the dipole axis, V points radially outward and is parallel to the magnetic equator, and D is eastward and completes a right-handed orthogonal system. For the 68 events, we examined whether magnetic fiel dipolarization appeared or not. A criterion of dipolarization is that ΔH increased by 20 nT in 5 min. From this event selection criterion, 17 events of magnetic fiel dipolarization in the deep inner magnetosphere were finall registered.

Figure 2 shows by circles (both fille and open) the MDS-1 location in the L-MLT plane for the 68 candidate events. The fille circles designate the 17 events of magnetic fiel dipolarization. We noticed that magnetic fiel dipolarization was often detected around L=5.5-6.5, though there are some events even at $L<5$. The number of selected events indicates that dipolarization can be found inside the geosynchronous orbit with an occurrence probability of 25% on average (=17/68) and is not an unusual phenomenon.

3.2. Example of Selected Events

Figure 3 displays the magnetic fiel variation data (ΔV, ΔD, and ΔH) for 3 dipolarization events covering a wide range of L (i.e., L=3.6-5.9), taken from the 17 selected events. They showed typical signatures of dipolarization in the deep inner magnetosphere. Figure 4 shows the Dst index around the onset time of dipolarization, which is indicated by a dot, for the 3 events.

3.2.1. 0028 UT on 19 March 2002 (Event 1)

Figure 3a shows a magnetic fiel dipolarization that occurred at 0028 UT on 19 March 2002. Auroral onset was found by *Frey et al.* [2004] at 0030:43 UT at MLT=23.2 hr. MDS-1 was located at L∼5.9 and MLT∼1.4 hr during the event. Note that ΔH started to decrease rapidly by ∼20 nT from ∼0026 UT, followed by an increase of ∼100 nT after 0028 UT. During the dipolarization, the magnetic fiel showed strong fluctuation whose period was much shorter than 1 min. From Figure 4a, we found that this event occurred in the main phase of a magnetic storm ($\text{Dst}_{min}=-37$ nT).

3.2.2. 0827 UT on 14 May 2002 (Event 2)

Figure 3b shows a magnetic fiel dipolarization that appeared in the deeper magnetosphere (L∼4.3 and MLT∼21.1 hr) at 0827 UT on 14 May 2002. Auroral onset was at 0826:26 UT at MLT=22.4 hr.

ΔH dropped sharply in a short time at 0826 UT and then increased by about 80 nT. This change in the magnetic fiel (i.e., a brief decrease in ΔH and subsequent dipolarization) is similar to that in Event 1. During dipolarization, the magnetic fiel was highly disturbed with short-period (much less than 1 min) fluctuations As shown in Figure 4b, this event also occurred in the main phase of a magnetic storm (Dst_{min}=−65 nT).

3.2.3. 0819 UT on 18 April 2002 (Event 3)

Figure 3c displays a magnetic fiel dipolarization that appeared in the innermost magnetosphere out of the selected 17 events. Since the MAM data before 0818:35 UT were recorded with the lowest resolution mode (mode 3) and had quantization noise, the data for 0800:00-0818:35 UT were smoothed by taking a moving average with an 11.5-sec time window. This dipolarization event was found at 0819 UT on 18 April 2002 at L∼3.6 and MLT∼22.2 hr. An associated auroral breakup was identifie at 0818:28 UT at MLT∼21.9 hr. The ΔH signature is similar to those of Events 1 and 2, that is, a rapid decrease followed immediately by dipolarization. In this event, ΔH decreased by ∼50 nT in 1 min (0818-0819 UT) and then showed a dipolarization signature of an increase of ∼150 nT. The magnetic fiel exhibited short-period fluctuation during dipolarization, in particular in the ΔV component. Figure 4c showed that this event fell in the main phase of a large magnetic storm (Dst_{min}=−124 nT).

3.3. Statistical Analysis

We examined the L-dependence of the occurrence probability of dipolarization. Figure 5a shows the distribution of L values of the MDS-1 satellite when auroral breakup occurred with $|\Delta MLT| \leq 2.5$ hr (i.e., 68 events). A peak appears at L=3.5-4.0, because of the orbital characteristics and seasonal dependence of the number of auroral breakups; that is, MDS-1 fl w at L=3.5-4.0 near midnight in February and March (see Figure 1), during which auroral onset was detected in large numbers than in April-July. The distribution of L values for the 17 selected dipolarization events is shown in Figure 5b. Gray shading represents the number of events during the storm main phase (like Events 1-3 in Figure 3). As shown in Figure 2, dipolarization can be seen at L=3.5-5.0, which has not been reported by previous studies. The occurrence probability is calculated from the number of dipolarization divided by the number of auroral breakups in each L bin; the result is shown in Figure 5c. Error bars represent 75% confidenc intervals that are calculated by using the maximum likelihood estimation [*Clopper and Pearson*, 1934]. The occurrence probability for storm-related dipolarization is shown with gray shading. We found that when the satellite is positioned close to auroral breakup meridian ($|\Delta MLT| \leq 2.5$ hr), dipolarization can be detected in ∼50% of events just inside the geosynchronous altitude (L=5.5-6.5) and in 7-38% of events in the deep inner magnetosphere (L=3.5-5.0). However, because of small number of the auroral breakups, ranges of the confidenc intervals are as wide as ∼±20%. Therefore, to increase the statistical significance we calculated the occurrence probability and the 75% confidenc interval over L=3.5-5.0 and L=5.5-6.5. Results were 16.1%(=5/31)±9.7% for L=3.5-5.0 and 50%(=12/24)±12.5% for L=5.5-6.5. It is important to note that a magnetic storm was developing whenever dipolarization was found at L=3.5-5.0, as indicated with gray shading.

3.4. Spectral Analysis

To examine the magnetic fiel fluctuation with periods much shorter than 1 min, we performed power spectral analysis. We took 10-minute segments of ΔV and ΔH during/before magnetic fiel dipolarization, and calculated their power spectra, which are shown in Figure 6 with solid/dotted black curves, respectively. Power spectra before dipolarization for Event 3 were not calculated, because of quantization noises due to the mode 3 observation (Figures 6e and 6f). Figures 6a-6d show that before dipolarization, the wave power decreases steeply in a period range of ≤100 sec. However, during dipolarization, the wave power was much enhanced and it was more significantl seen in a period range around 10 sec or possibly shorter. We also noticed that the slopes of power spectra during dipolarization change around a period of 3-5 sec in ΔV for all events (Figures 6a, 6c, and 6e) and in ΔH for Event 1 and 2 (Figures 6b and 6d). For visual aid, a red dotted line is fitte to the power spectrum in the portion of longer period (10-200 sec). It can be seen that the power spectra lie below the red dotted line around a period of 1 sec; in other words, the slopes become steeper in the period range shorter than ∼5 sec in Events 1 and 3, and ∼3 sec in Event 2. This indicates that magnetic fiel fluctuation during dipolarization in the deep inner magnetosphere have a characteristic timescale (T_C) of several seconds, around which the spectral slopes change. The characteristic timescale is rather consistent with those reported by previous studies: T_C=0.3-10 sec at r=7-9 R_E [*Lui et al.*, 1992], T_C>3 sec at r=7-9 R_E [*Ohtani et al.*, 1995], T_C=8-28 sec at r∼8 R_E [*Ohtani et al.*, 1998], and T_C∼5 sec at X=−8 to −11 R_E [*Shiokawa et al.*, 2005].

We compared the characteristic timescale with an ion gyroperiod (T_G). Table 1 summarizes the results. The third column gives the T_C values from Figure 6. In the fourth column, the magnitude of the magnetic fiel measured by MDS-1/MAM ($B_{measured}$) is presented, where the magnitude is given by an average value during the 10-minute interval of dipolarization adopted for power spectrum calculation (Figure 6). The next two columns indicate gyroperiods of H^+ and O^+ ions derived from $2\pi m/eB_{measured}$, where m is the ion mass and e is the electric charge. The last two columns are the ratios of T_G/T_C for H^+ and O^+ ions. We noticed that T_G/T_C for H^+ is 0.03-0.20 and rather smaller than 1. *Ohtani et al.* [1995, 1998] found that T_G/T_C for H^+ is 0.08-0.3 at r∼8 R_E, which is similar to the present result. On the other hand, T_G/T_C for O^+ is 0.5-3.3 and comparable to 1. Thus, we suppose that the magnetic fiel fluctuations during dipolarization have a nonadiabatic effect (probably acceleration) on O^+ ions.

4. Analysis of IMAGE/HENA Data

4.1. Example of ENA Images (Event 3)

In section 3, we found that dipolarization in the deep inner magnetosphere occurred in the main phase of a magnetic storm and was accompanied by magnetic fiel fluctuation with periods of several seconds. It was also suggested that the fluctuation may accelerate O^+ ions in a nonadiabatic way. Therefore, we investigated the response of H^+ and O^+ ions during dipolarization by analyzing ENA images obtained by the IMAGE satellite.

Figure 7 shows an example of the IMAGE/HENA images during the dipolarization occuring at 0819 UT on 18 April 2002 (Event 3). Top and bottom panels display ENA images of hydrogen in an energy range of 60-198 keV and oxygen in an energy range of 52-180 keV, respectively, at four different time intervals (0730-0740 UT, 0800-0810 UT, 0830-0840 UT, and 0900-0910 UT). These ENA energy ranges cover the main portion of the ring current energy [*Williams*, 1981]. The dipolarization was initiated between the second and third images. In each image, the dipole magnetic fiel lines at 0000, 0600, 1200, and 1800 MLT are drawn for L values of 4 and 8. Dotted lines designate the grid of instrumental coordinates, that is, the polar direction (from bottom-left to top-right) and azimuthal direction (from bottom-right to top-left). A cut-off in ENA flu on the dayside over ∼60° azimuth was caused by the shutter on the HENA imager that protects the detectors from direct sunlight. Since the IMAGE satellite was located at high latitude on the nightside ((X, Y, Z)∼(−3.0, 1.8, 7.2) R_E in solar-magnetic coordinates), a line-of-sight to a given grid in the inner magnetosphere become the closest to the Earth near the equatorial plane, where the geocorona density is high and the charge exchange process occurs frequently. Thus we can consider that ENAs were generated in the vicinity of the geomagnetic equator in the deep inner magnetosphere.

We noticed that after dipolarization, the hydrogen ENA flu on the nightside increased slightly, whereas the oxygen ENA flu on

the nightside was greatly enhanced, suggesting mass-dependent acceleration of ions at dipolarization. Note that the oxygen ENA flu stayed at a higher level even at 0900-0910 UT, when the dipolarization had already ended (Figure 4c).

4.2. ENA Flux Variation of Selected Events

To examine the temporal variations in ENA flu in more detail for the selected 3 dipolarization events, we calculated the ENA flu integrated over the nightside ring current area. The integrated area is confine to a polar angle of $\pm 36°$ and an azimuthal angle of $-36°$ to $0°$ excluding the near-Earth area (i.e., a polar angle of $\pm 18°$ and an azimuthal angle of $-18°$ to $0°$), that is, a "backward C-shaped" area outlined in red in the top-leftmost panel of Figure 7. The near-Earth flu must be excluded, because it comes from mirroring ions that originate from larger L and interact with the dense neutral atmosphere at low altitude [*Mitchell et al.*, 2003]. Then we computed the normalized flu ($J_{normalized}$) from the integrated flu derived above ($J_{integrated}$), as it is measured at a radial distance of 8 R_E, by

$$J_{normalized} = (r/8)^2 \times J_{integrated},$$

where, r is the radial distance of the satellite position in R_E. In this equation, we expect that the ENA flu decreases with radial distance roughly as $1/r^2$ [*Ohtani et al.*, 2006]. The above procedure is applied to a series of original ENA images that have a time resolution of 2 min. The normalized ENA flu is considered as a proxy of ring current intensity around r=3-6 R_E on the nightside, though it may contain small uncertainties caused by variations of the pitch angle distribution of ring current ions [*C:son Brandt et al.*, 2002a; *Keika et al.*, 2006], the effective angular resolution of ENA images [*Mitchell et al.*, 2003; *Ohtani et al.*, 2006], and a motion of the IMAGE satellite [*Ohtani et al.*, 2005].

4.2.1. 0028 UT on 19 March 2002 (Event 1)

Figure 8a shows the normalized ENA flu around the dipolarization observed at 0028 UT on 19 March 2002. Red and blue lines denote hydrogen and oxygen ENA flu es, respectively. The hydrogen flu showed no change during dipolarization, while the oxygen flu was clearly enhanced by a factor of $\sim$5 (from 1×10^2 (cm^2 sr s)$^{-1}$ to 5×10^2 (cm^2 sr s)$^{-1}$) at almost the same time as the dipolarization. The oxygen flu remained constant for at least 1.5 hr after the dipolarization.

4.2.2. 0827 UT on 14 May 2002 (Event 2)

Figure 8b gives $J_{normalized}$ of hydrogen and oxygen for the dipolarization observed at 0827 UT on 14 May 2002. Both the hydrogen and oxygen ENA flu es started to increase around 0827 UT. The increase was more significan for oxygen than for hydrogen; the oxygen flu changed by a factor of $\sim$4 (from 2.5×10^2 (cm^2 sr s)$^{-1}$ to 1×10^3 (cm^2 sr s)$^{-1}$), and hydrogen by a factor of $\sim$1.5 (from 2×10^4 (cm^2 sr s)$^{-1}$ to 3×10^4 (cm^2 sr s)$^{-1}$). The oxygen flu remained at 1×10^3 (cm^2 sr s)$^{-1}$ for 1 hr.

4.2.3. 0819 UT on 18 April 2002 (Event 3)

Figure 8c shows $J_{normalized}$ of hydrogen and oxygen for the dipolarization observed at 0819 UT on 18 April 2002. We found that the oxygen ENA flu increased more clearly than the hydrogen ENA flux which is also seen in Figure 7. The enhancement factor was $\sim$2 for oxygen (from 1.5×10^3 (cm^2 sr s)$^{-1}$ to 3×10^3 (cm^2 sr s)$^{-1}$) and $\sim$1.2 for hydrogen (from 2.5×10^4 (cm^2 sr s)$^{-1}$ to 3×10^4 (cm^2 sr s)$^{-1}$). As in Events 1 and 2, the oxygen ENA flu was remained at an enhanced level for more than 1 hr.

4.3. Spatiality of Acceleration Site

From Figures 7 and 8, we found that after dipolarization, the oxygen ENA flu was more strongly enhanced than the hydrogen ENA flu and stayed at a higher level for $\geq$1 hr. The maintenance of the higher oxygen ENA flu implies that the acceleration of O^+ ions occurred over a broader region rather than a limited region, so that the ring current on the nightside is replenished continuously by accelerated ions. This implication is consistent with azimuthal and radial propagation of magnetic fiel dipolarization which has been found outside the geosynchronous orbit by previous studies (see section 1). Thus we suggest that the dipolarization initiated in the deep inner magnetosphere also extends out to a certain degree and provides nonadiabatic acceleration of O^+ ions over a spatially wide area.

5. Discussion

In this section, we firs answer the following 4 questions regarding dipolarization in the inner magnetosphere (r<6.6 R_E), which were raised in the Introduction: (1) how deep can dipolarization be detected?; (2) how frequently can dipolarization be observed in the deep inner magnetosphere?; (3) does dipolarization in the deep inner magnetosphere show similar signatures to that at $r\geq$6.6 R_E?; and (4) does dipolarization in the deep inner magnetosphere contribute to ion acceleration and ring current formation? Then, a new scenario of energization and transport of O^+ ions will be described together with previous scenarios. Finally, we will discuss remaining issues.

5.1. Answers to Target Questions

For the firs question, we found answers in Figures 2, 3, and 5. Dipolarization can be detected over a wide range of L (i.e., L=3.5-6.5). It was surprising that the MDS-1 satellite observed local dipolarization in the ring current region (L=3.5-5.0). Such a report of dipolarization in the ring current region (or in the deep inner magnetosphere) has never been made in previous studies and will shed a new light on development mechanisms of the ring current, as discussed later.

An answer to the second question can be found in Figure 5. When the satellite was positioned close to the auroral breakup meridian ($|\Delta$MLT$|\leq$2.5 hr), the occurrence probability was about 50% just inside the geosynchronous altitude. Even if the satellite moved further inside at L=3.5-5.0, the occurrence probability is still as high as $\sim$16%. This result suggests that magnetic fiel dipolarization in the deep inner magnetosphere is not uncommon phenomenon.

Figures 3 and 6 provide answers to the third question. In all of 3 events, ΔH decreased shortly by 5-50 nT just before dipolarization (Figure 3). This transient decrease of ΔH before dipolarization has been reported by previous studies using the GOES and AMPTE/CCE satellites and is called "the explosive growth phase" [e.g., *Ohtani et al.*, 1991, 1992b]. From Figure 6 we found that magnetic fiel fluctuation with a characteristic timescale of 3-5 sec accompanied dipolarization. This characteristic timescale is in the period range ($\sim$3-30 sec) of fluctuation observed at r=7-11 R_E [*Lui et al.*, 1992; *Ohtani et al.*, 1995, 1998; *Shiokawa et al.*, 2005]. Therefore, we conclude that magnetic fiel signatures found in the deep inner magnetosphere (i.e., transient depression and fluctua tions with 3-5 sec timescale) are consistent with those found outside the geosynchronous altitude.

The last question is answered with Table 1 as well as Figures 4, 7, and 8. We found that dipolarization in the deep inner magnetosphere is accompanied by magnetic fiel fluctuation with a characteristic timescale of several seconds. The characteristic timescale is almost comparable with the gyroperiod of O^+ ions ($T_G(O^+)/T_C\sim$1), while it is rather longer than the gyroperiod of H^+ ions ($T_G(H^+)/T_C<$1). Therefore, the firs adiabatic invariant of O^+ ions will be violated, and they will be accelerated nonadiabatically. Such an acceleration mechanism has also been proposed by *Ono et al.* [2009], who found that ions are accelerated by the electric fiel induced by magnetic fiel fluctuation whose characteristic timescale is close to the ion gyroperiod. On the other hand, H^+ ions will not be accelerated effectively, because the fluctuation will not be able to violate the H^+ firs adiabatic invariant. From a test particle simulation, *Artemyev et al.* [2009] found that particles are accelerated similarly by interaction with turbulent electromagnetic fiel in the current sheet. The above expectation is justifie

by the ENA observations shown in Figures 7 and 8. That is, magnetic fiel dipolarization is followed by ENA flu enhancement in the nightside ring current region. In particular, oxygen ENA flu was predominantly enhanced by a factor of 2-5 and remained at an enhanced level for more than 1 hr. The ENA observation leads us to consider that high-energy O^+ ions were generated in the ring current region and became an important constituent of the ring current plasma. This idea is supported by Figure 4, in which the dipolarization events were associated with the main phase of geomagnetic storms, that is, augmentation of the ring current. From the discussion above, we suppose that dipolarization in the deep inner magnetosphere plays a crucial role in acceleration of O^+ ions and development of the O^+-rich ring current.

5.2. Generation Scenario for O^+-rich Ring Current

Previous studies based on in situ measurement reported that the ion composition of the ring current changes drastically during magnetic storms. Although H^+ ions are a dominant component in the inner magnetosphere during quiet periods, O^+ ions come to provide more than ∼50% of the total ring current energy during storm main phase [e.g., *Hamilton et al.*, 1988; *Roeder et al.*, 1996; *Daglis*, 1997; *Daglis et al.*, 2000]. Some scenarios have been proposed to explain this strong enhancement of O^+ energy density in the ring current. Figure 9 schematically summarized the proposed scenarios.

In the firs scenario (scenario I in Figure 9), O^+ ions are transported directly from the ionosphere to the ring current and are accelerated up to a few tens of keV on their way. *Daglis et al.* [1994] performed a numerical calculation of O^+ ion trajectories during fiel reconfiguration and found that 3.2 keV O^+ ions launched from the auroral latitude reached the geomagnetic equator around r=7-8 R_E with a fina energy of 50-70 keV within a few minutes. *Gazey et al.* [1996] examined a conjunction event of the CRRES satellite with the EISCAT radar, and concluded that O^+ injections observed at substorm onset at L∼6 were coming directly from auroral arcs. Analyzing ion data from the Polar satellite, *Sheldon et al.* [1998] speculated that oxygen ions are extracted and accelerated up to ∼40 keV by a parallel electric fiel generated by storm injection.

The firs half of the second and third scenarios (scenarios II and III in Figure 9) is the same: O^+ ions are extracted from the polar ionosphere, travel through the magnetic lobes, and then are transported into the plasma sheet. In the second half of scenario II, O^+ ions in the near-Earth plasma sheet are convected into the ring current by the dawn-to-dusk electric fiel and are accelerated simultaneously by betatron acceleration. *Lui et al.* [1986] and *Lui* [1993] found that the phase space density of oxygen ions at $L \leq 5$ during the main phase is almost the same as that at L=5.5-8.5 during the prestorm, indicating inward radial displacement of ions by an enhanced convection. Recent numerical simulation studies coupling the global MHD code (LFM/BATS-R-US) with the convection code (CRCM/RCM) implicitly include adiabatic transport of ions from the near-Earth plasma sheet (r=8-10 R_E) into the inner magnetosphere [e.g., *De Zeeuw et al.*, 2004; *Fok et al.*, 2006; *Moore et al.*, 2007].

However, in the second half of scenario III, O^+ ions in the near-Earth plasma sheet experience abrupt nonadiabatic acceleration and transport into the ring current due to an impulsive electric fiel associated with dipolarization. This mechanism is proposed with numerical calculation of ion trajectories by *Delcourt et al.* [1990], *Sánchez et al.* [1993], *Delcourt* [2002], and *Jones et al.* [2006], and is favored with ENA observations by *C:son Brandt et al.* [2002b], *Mitchell et al.* [2003], and *Ohtani et al.* [2005]. ENA imaging has been used to study how the plasmasheet and ring current responds during substorms and how that relates to dipolarizations. *C:son Brandt et al.* [2002b] analyzed ENA images obtained by IMAGE/HENA and found that the ENA intensities from the plasmasheet outside about 8 R_E decrease suddenly at substorm onset, probably indicative of an earthward propagating dipolarization front. *Mitchell et al.* [2003] and *Ohtani et al.* [2005] demonstrated that the O-ENA intensities enhance abruptly at substorm onset and the intensificatio lasts 30-60 min. The H-ENA intensities enhance much more gradually. They suggested that this supports nonadiabatic acceleration of O^+ ions by an impulsive electric fiel during the dipolarization process.

In addition to the above three scenarios, in the present study, we propose another plausible scenario (scenario IV in Figure 9). It is known from previous studies employing the DE-1 satellite that a large amount of thermal O^+ ions exists in the outer plasmasphere (L=2.0-5.0) [*Horwitz et al.*, 1984; *Roberts et al.*, 1987; *Comfort et al.*, 1988; *Fraser et al.*, 2005], which is called "the oxygen torus". These thermal O^+ ions can be frequently observed even in low Kp periods (Kp=0-2+) in the late evening hours [*Roberts et al.*, 1987]. The MDS-1/MAM data showed that dipolarization can be observed in the ring current region (i.e., L=3.5-5.0) and the IMAGE/HENA data suggested that dipolarization causes strong enhancement of O^+ ion flu and ring current development. Thus, we presume that the preexisting thermal O^+ ions in the oxygen torus are locally and nonadiabatically accelerated by fluctuation associated with dipolarization in the deep inner magnetosphere, resulting in formation of the O^+-rich ring current.

As shown above, recent numerical and observational studies mostly accommodate scenario II or III; however, we here conjecture that when the dipolarization extends in as far as L∼3.5, acceleration of the local thermal O^+ population may also contribute, as described in our scenario IV. In the actual magnetosphere, combination of some of these four scenarios may play an important role on the O^+-rich ring current development, rather than that only one of them takes effect. In further studies we need to identify relative importance among scenarios I-IV for the O^+-rich ring current development.

5.3. Remaining Issues

This study raised for the firs time the possibility that local nonadiabatic acceleration of O^+ ions in the deep inner magnetosphere (L=3.5-5.0) during dipolarization is more important for the formation of the ring current as well as its ion composition change than ever considered. However, two remaining issues must be examined. First, it is yet unclear whether fluctuation of the geomagnetic fiel during dipolarization have enough energy to accelerate thermal O^+ ions up to the ring current energy (a few tens to a few hundreds of keV). Second, it is of interest to examine what mechanisms determine the characteristic timescale of the magnetic fluctuation to be several seconds. It might be difficul to fin answers for these issues with the present data set, because the MDS-1 satellite is a single satellite and unfortunately did not carry instruments to measure the electric fiel and ion differential flux Future satellite missions such as Energization and Radiation in Geospace (ERG) in Japan and Radiation Belt Storm Probe (RBSP) in the US, which plan to measure the magnetic and electric field along with energetic ion flu and ion composition at multiple locations in the inner magnetosphere, would give clues to solving these issues.

6. Summary

We studied magnetic fiel reconfiguratio and associated ion acceleration in the deep inner magnetosphere, using magnetic fiel data obtained by the MDS-1 satellite and the high-energetic neutral atom flu data obtained by the IMAGE satellite for the period of February to July in 2002. Out of 68 events in which substorms were identifie by IMAGE/FUV auroral images and the MDS-1 satellite was located at L=3.0-6.5 near the auroral onset longitude ($|\Delta MLT| \leq 2.5$ hr), 17 events of magnetic fiel dipolarization were identifie in the deep inner magnetosphere. The overall occurrence probability is 25% (=17/68). If we limit events to those just inside the geosynchronous altitude (L=5.5-6.5) and in the deep inner magnetosphere (L=3.5-5.0), the occurrence probability becomes ∼50% and ∼16%, respectively. Surprisingly, we found an event at L∼3.6, far inside the geosynchronous altitude. This suggests that magnetic fiel dipolarization in the deep inner magnetosphere is not uncommon. We also found that a magnetic storm was developing when

dipolarization was found at L=3.5-5.0. This implies that it is difficul to fin dipolarization signatures in the deep inner magnetosphere during nonstorm period.

Spectral analysis was performed for 3 typical dipolarization events. Slope of power spectrum was changed at a period of 3-5 sec. This indicates that the magnetic fiel fluctuation during dipolarization in the deep inner magnetosphere have a characteristic timescale (T_C) of several seconds. Comparison of the characteristic timescale with the ion gyroperiod (T_G) revealed that T_G/T_C for H^+ is 0.03-0.20 (<1) and T_G/T_C for O^+ is 0.5-3.3 (≈ 1). These results lead us to consider that the magnetic fiel fluctuation cause nonadiabatic acceleration of O^+ ions. To test this idea, we investigated the response of H^+ and O^+ ions during the 3 dipolarization events by analyzing HENA images obtained by the IMAGE satellite. We found that the oxygen ENA flu in the nightside ring current region was greatly increased by a factor of 2-5, whereas the hydrogen ENA flu in the same region showed insignifican enhancement. After dipolarization, the oxygen ENA flu was maintained at an enhanced level for more than 1 hr.

It is well-known that the ion composition of the ring current changes drastically during magnetic storms. Although H^+ ions are the dominant component in the inner magnetosphere during quiet periods, O^+ ions contribute by more than $\sim$50% to the total ring current energy during storm main phase. Several scenarios have been proposed to understand the O^+-rich ring current generation (see Figure 9): (1) direct transport of O^+ ions from the ionosphere to the ring current, (2) transport of O^+ ions in the pathway of "ionosphere, magnetic lobe, near-Earth plasma sheet" followed by adiabatic transport into the ring current and betatron acceleration, and (3) transport of O^+ ions in the pathway of "ionosphere, magnetic lobe, near-Earth plasma sheet" followed by nonadiabatic transport and acceleration by an inductive electric fiel due to dipolarization. However, based on the present observational results, we presumed another plausible scenario: thermal O^+ ions preexist in the outer plasmasphere (L=2.0-5.0) during quiet intervals and they are locally and nonadiabatically accelerated by fluctuation associated with dipolarization in the deep inner magnetosphere, resulting in the O^+-rich ring current. Local acceleration of O^+ ions in the deep inner magnetosphere (L=3.5-5.0) may be more important for ring current development than ever considered.

Acknowledgements

We thank D. G. Mitchell for his help in processing the IMAGE/HENA data. The list of auroral breakups observed by IMAGE/FUV is provided by H. U. Frey. The Dst index is provided by World Data Center for Geomagnetism, Kyoto. We are thankful to T. Nagai, S. Ohtani, and G. Ueno for their helpful comments. This work was supported by the Kurata Memorial Hitachi Science and Technology Foundation (grant 844), the Japan Securities Scholarship Foundation (grant 1368), Inamori Foundation, ISM Cooperative Research Program, and the Ministry of Education, Science, Sports and Culture, Grant-in-Aid for Young Scientists (B) (grants 19740303 and 22740322).

References

Angelopoulos, V. (2008), The THEMIS Mission, *Space Sci. Rev.*, *141*, 5–34, doi:10.1007/s11214-008-9336-1.

Artemyev, A. V., L. M. Zelenyi, H. V. Malova, G. Zimbardo, and D. Delcourt (2009), Acceleration and transport of ions in turbulent current sheets: formation of non-maxwelian energy distribution, *Nonlin. Processes Geophys.*, *16*, 631–639.

Burch, J. L. (2000), IMAGE mission overview, *Space Sci. Rev.*, *91*, 1–14.

Clopper, C. J., and E. S. Pearson (1934), The use of confidenc or fiducia limits illustrated in the case of the binomial, *Biometrika*, *26*(4), 404–413.

Comfort, R. H., I. T. Newberry, and C. R. Chappell (1988), Preliminary statistical survey of plasmaspheric ion properties from observations by DE 1/RIMS, in *Modeling Magnetospheric Plasma*, *Geophys. Monogr. Ser.*, vol. 44, edited by T. E. Moore and J. J. H. Waite, pp. 107–114, AGU, Washington, D.C.

C:son Brandt, P., E. C. Roelof, S. Ohtani, D. G. Mitchell, and B. Anderson (2002a), IMAGE/HENA: pressure and current distributions during the 1 October 2002 storm, *Adv. Space Res.*, *33*, 719–722, doi:10.1016/S0273-1177(03)00633-1.

C:son Brandt, P., R. Demajistre, E. C. Roelof, S. Ohtani, D. G. Mitchell, and S. Mende (2002b), IMAGE/high-energy energetic neutral atom: Global energetic neutral atom imaging of the plasma sheet and ring current during substorms, *J. Geophys. Res.*, *107*, 1454, doi:10.1029/2002JA009307.

Cummings, W. D., J. N. Barfield and P. J. Coleman, Jr. (1968), Magnetospheric substorms observed at the synchronous orbit, *J. Geophys. Res.*, *73*, 6687–6698, doi:10.1029/JA073i021p06687.

Daglis, I. A. (1997), The role of magnetosphere-ionosphere coupling in magnetic storm dynamics, in *Magnetic Storms*, *Geophys. Monogr. Ser.*, vol. 98, edited by B. T. Tsurutani, pp. 107–116, AGU, Washington, D.C.

Daglis, I. A., M. Banaszkiewicz, and E. B. Wodnicka (1994), Coupling of the high-latitude and the equatorial magnetosphere during substorms through the transport/acceleration of ionospheric ions, *Proceedings Int. Conf. Substorms-2*, pp. 615–619.

Daglis, I. A., Y. Kamide, C. Mouikis, G. D. Reeves, E. T. Sarris, K. Shiokawa, and B. Wilken (2000), "Fine Structure" of the Storm-Substorm Relationship: Ion Injections During Dst Decrease, *Adv. Space Res.*, *25*, 2369–2372, doi:10.1016/S0273-1177(99)00525-6.

De Zeeuw, D. L., S. Sazykin, R. A. Wolf, T. I. Gombosi, A. J. Ridley, and G. Tóth (2004), Coupling of a global MHD code and an inner magnetospheric model: Initial results, *J. Geophys. Res.*, *109*, A12219, doi:10.1029/2003JA010366.

Delcourt, D. C. (2002), Particle acceleration by inductive electric field in the inner magnetosphere, *J. Atmos. Sol. Terr. Phys.*, *64*, 551–559, doi:10.1016/S1364-6826(02)00012-3.

Delcourt, D. C., A. Pedersen, and J. A. Sauvaud (1990), Dynamics of single-particle orbits during substorm expansion phase, *J. Geophys. Res.*, *95*, 20,853–20,865, doi:10.1029/JA095iA12p20853.

Fok, M., T. E. Moore, P. C. Brandt, D. C. Delcourt, S. P. Slinker, and J. A. Fedder (2006), Impulsive enhancements of oxygen ions during substorms, *J. Geophys. Res.*, *111*, A10222, doi:10.1029/2006JA011839.

Fraser, B. J., J. L. Horwitz, J. A. Slavin, Z. C. Dent, and I. R. Mann (2005), Heavy ion mass loading of the geomagnetic fiel near the plasmapause and ULF wave implications, *Geophys. Res. Lett.*, *32*, L04102, doi:10.1029/2004GL021315.

Frey, H. U., S. B. Mende, V. Angelopoulos, and E. F. Donovan (2004), Substorm onset observations by IMAGE-FUV, *J. Geophys. Res.*, *109*, A10304, doi:10.1029/2004JA010607.

Fu, S. Y., Q. G. Zong, T. A. Fritz, Z. Y. Pu, and B. Wilken (2002), Composition signatures in ion injections and its dependence on geomagnetic conditions, *J. Geophys. Res.*, *107*, 1299, doi:10.1029/2001JA002006.

Gazey, N. G. J., et al. (1996), EISCAT/CRRES observations: nightside ionospheric ion outfl w and oxygen-rich substorm injections, *Ann. Geophys.*, *14*, 1032–1043, doi:10.1007/s005850050364.

Hamilton, D. C., G. Gloeckler, F. M. Ipavich, B. Wilken, and W. Stuedemann (1988), Ring current development during the great geomagnetic storm of February 1986, *J. Geophys. Res.*, *93*, 14,343–14,355, doi:10.1029/JA093iA12p14343.

Heppner, J. P., M. Sugiura, T. L. Skillman, B. G. Ledley, and M. Campbell (1967), OGO-A magnetic fiel observations, *J. Geophys. Res.*, *72*, 5417–5471, doi:10.1029/JZ072i021p05417.

Horwitz, J. L., R. H. Comfort, and C. R. Chappell (1984), Thermal ion composition measurements of the formation of the new outer plasmasphere and double plasmapause during storm recovery phase, *Geophys. Res. Lett.*, *11*, 701–704, doi:10.1029/GL011i008p00701.

Jacquey, C., J. A. Sauvaud, and J. Dandouras (1991), Location and propagation of the magnetotail current disruption during substorm expansion - Analysis and simulation of an ISEE multi-onset event, *Geophys. Res. Lett.*, *18*, 389–392, doi:10.1029/90GL02789.

Jones, S. T., M. Fok, and P. C. Brandt (2006), Modeling global O+ substorm injection using analytic magnetic fiel model, *J. Geophys. Res.*, *111*, A11S07, doi:10.1029/2006JA011607.

Keika, K., M. Nosé, P. C. Brandt, S. Ohtani, D. G. Mitchell, and E. C. Roelof (2006), Contribution of charge exchange loss to the storm time ring current decay: IMAGE/HENA observations, *J. Geophys. Res.*, *111*, A11S12, doi:10.1029/2006JA011789.

Koshiishi, H., Y. Kimoto, H. Matumoto, K. Ueno, and T. Goka (2004), Space environment data acquisition equipment on board Tsubasa satellite, *Space Radiation*, *4*(2), 73–80.

Lopez, R. E., and A. T. Y. Lui (1990), A multisatellite case study of the expansion of a substorm current wedge in the near-earth magnetotail, *J. Geophys. Res.*, *95*, 8009–8017, doi:10.1029/JA095iA06p08009.

Lopez, R. E., A. T. Y. Lui, D. G. Sibeck, R. W. McEntire, L. J. Zanetti, T. A. Potemra, and S. M. Krimigis (1988), The longitudinal and radial distribution of magnetic reconfiguration in the near-earth magnetotail as observed by AMPTE/CCE, *J. Geophys. Res.*, *93*, 997–1001, doi:10.1029/JA093iA02p00997.

Lui, A. T. Y. (1993), Radial transport of storm time ring current ions, *J. Geophys. Res.*, *98*, 209–214, doi:10.1029/92JA02079.

Lui, A. T. Y. (2001), Current controversies in magnetospheric physics, *Rev. Geophys.*, *39*, 535–564, doi:10.1029/2000RG000090.

Lui, A. T. Y., R. W. McEntire, S. M. Krimigis, and E. P. Keath (1986), Acceleration of energetic oxygen ($E>137$ keV) in the storm-time ring current, in *Ion Acceleration in the Magnetosphere and Ionosphere*, *Geophys. Monogr. Ser.*, vol. 38, edited by T. Chang, pp. 149–152, AGU, Washington, D.C.

Lui, A. T. Y., et al. (1992), Current disruptions in the near-earth neutral sheet region, *J. Geophys. Res.*, *97*, 1461–1480, doi:10.1029/91JA02401.

Maynard, N. C., W. J. Burke, E. M. Basinska, G. M. Erickson, W. J. Hughes, H. J. Singer, A. G. Yahnin, D. A. Hardy, and F. S. Mozer (1996), Dynamics of the inner magnetosphere near times of substorm onsets, *J. Geophys. Res.*, *101*, 7705–7736, doi:10.1029/95JA03856.

McPherron, R. L., M. P. Aubry, C. T. Russell, and P. J. Coleman, Jr. (1973), Satellite studies of magnetospheric substorms on August 15, 1968. 4. Ogo 5 magnetic fiel observations, *J. Geophys. Res.*, *78*, 3068–3078, doi:10.1029/JA078i016p03068.

Mitchell, D. G., et al. (2000), High energy neutral atom (HENA) imager for the IMAGE mission, *Space Sci. Rev.*, *91*, 67–112.

Mitchell, D. G., P. C:Son Brandt, E. C. Roelof, D. C. Hamilton, K. C. Retterer, and S. Mende (2003), Global imaging of O^+ from IMAGE/HENA, *Space Sci. Rev.*, *109*, 63–75, doi:10.1023/B:SPAC.0000007513.55076.00.

Moore, T. E., M. Fok, D. C. Delcourt, S. P. Slinker, and J. A. Fedder (2007), Global aspects of solar wind ionosphere interactions, *J. Atmos. Sol. Terr. Phys.*, *69*, 265–278, doi:10.1016/j.jastp.2006.08.009.

Nagai, T. (1982), Observed magnetic substorm signatures at synchronous altitude, *J. Geophys. Res.*, *87*(A6), 4405–4417.

Ohtani, S. (1998), Earthward expansion of tail current disruption: Dual-satellite study, *J. Geophys. Res.*, *103*, 6815–6826, doi:10.1029/98JA00013.

Ohtani, S., K. Takahashi, L. J. Zanetti, T. A. Potemra, R. W. McEntire, and T. Iijima (1991), Tail current disruption in the geosynchronous region, in *Magnetospheric Substorms*, *Geophys. Monogr. Ser.*, vol. 64, edited by J. R. Kan, T. A. Potemra, S. Kokubun, and T. Iijima, pp. 131–137, AGU, Washington, D.C.

Ohtani, S., S. Kokubun, and C. T. Russell (1992a), Radial expansion of the tail current disruption during substorms - A new approach to the substorm onset region, *J. Geophys. Res.*, *97*, 3129–3136, doi:10.1029/91JA02470.

Ohtani, S., K. Takahashi, L. J. Zanetti, T. A. Potemra, R. W. McEntire, and T. Iijima (1992b), Initial signatures of magnetic fiel and energetic particle flu es at tail reconfiguratio - Explosive growth phase, *J. Geophys. Res.*, *97*, 19,311–19,324, doi:10.1029/92JA01832.

Ohtani, S., T. Higuchi, A. T. Y. Lui, and K. Takahashi (1995), Magnetic fluctuation associated with tail current disruption: Fractal analysis, *J. Geophys. Res.*, *100*, 19,135–19,146, doi:10.1029/95JA00903.

Ohtani, S., K. Takahashi, T. Higuchi, A. T. Y. Lui, H. E. Spence, and J. F. Fennell (1998), AMPTE/CCE-SCATHA simultaneous observations of substorm-associated magnetic fluctuations *J. Geophys. Res.*, *103*, 4671–4682, doi:10.1029/97JA03239.

Ohtani, S., P. C. Brandt, D. G. Mitchell, H. Singer, M. Nosé, G. D. Reeves, and S. B. Mende (2005), Storm-substorm relationship: Variations of the hydrogen and oxygen energetic neutral atom intensities during storm-time substorms, *J. Geophys. Res.*, *110*, A07219, doi:10.1029/2004JA010954.

Ohtani, S., P. C. Brandt, H. J. Singer, D. G. Mitchell, and E. C. Roelof (2006), Statistical characteristics of hydrogen and oxygen ENA emission from the storm-time ring current, *J. Geophys. Res.*, *111*, A06209, doi:10.1029/2005JA011201.

Ohtani, S., et al. (2007), Cluster observations in the inner magnetosphere during the 18 April 2002 sawtooth event: Dipolarization and injection at r=4.6 R_E, *J. Geophys. Res.*, *112*(A11), A08213, doi:10.1029/2007JA012357.

Ono, Y., M. Nosé, S. Christon, and A. T. Y. Lui (2009), The role of magnetic fiel fluctuation in nonadiabatic acceleration of ions during dipolarization, *J. Geophys. Res.*, *114*, A05209, doi:10.1029/2008JA013918.

Roberts, W. T., Jr., J. L. Horwitz, R. H. Comfort, C. R. Chappell, J. H. Waite, Jr., and J. L. Green (1987), Heavy ion density enhancements in the outer plasmasphere, *J. Geophys. Res.*, *92*, 13,499–13,512, doi:10.1029/JA092iA12p13499.

Roeder, J. L., J. F. Fennell, M. W. Chen, M. Schulz, M. Grande, and S. Livi (1996), CRRES observations of the composition of the ring-current ion populations, *Adv. Space Res.*, *17*, 17–24, doi:10.1016/0273-1177(95)00689-C.

Sánchez, E. R., B. H. Mauk, and C. Meng (1993), Adiabatic vs. non-adiabatic particle distributions during convection surges, *Geophys. Res. Lett.*, *20*, 177–180, doi:10.1029/93GL00237.

Sergeev, V. A., M. A. Shukhtina, R. Rasinkangas, A. Korth, G. D. Reeves, H. J. Singer, M. F. Thomsen, and L. I. Vagina (1998), Event study of deep energetic particle injections during substorm, *J. Geophys. Res.*, *103*, 9217–9234, doi:10.1029/97JA03686.

Sheldon, R. B., H. E. Spence, and J. F. Fennell (1998), Observation of the 40 keV field-aligne ion beams, *Geophys. Res. Lett.*, *25*, 1617–1620, doi:10.1029/98GL01054.

Shiokawa, K., I. Shinohara, T. Mukai, H. Hayakawa, and C. Z. Cheng (2005), Magnetic fiel fluctuation during substorm-associated dipolarizations in the nightside plasma sheet around $X=-10R_E$, *J. Geophys. Res.*, *110*, A05212, doi:10.1029/2004JA010378.

Sugiura, M., T. L. Skillman, B. G. Ledley, and J. P. Heppner (1968), Propagation of the sudden commencement of July 8, 1966, to the magnetotail, *J. Geophys. Res.*, *73*, 6699–6709, doi:10.1029/JA073i021p06699.

Williams, D. J. (1981), Ring current composition and sources - An update, *Planet. Space Sci.*, *29*, 1195–1203, doi:10.1016/0032-0633(81)90124-0.

Table 1. Comparison between the characteristic timescale of magnetic fiel fluctuation (T_C) and ion gyroperiods (T_G).

Date (Event No.)	L	T_C (s)	$B_{measured}$ (nT)	$T_G(H^+)$ (s)	$T_G(O^+)$ (s)	$T_G(H^+)/T_C$	$T_G(O^+)/T_C$
2002/03/19 (Event 1)	5.9	∼5	64	1.02	16.35	∼0.20	∼3.27
2002/05/14 (Event 2)	4.3	∼3	274	0.24	3.83	∼0.08	∼1.28
2002/04/18 (Event 3)	3.6	∼5	394	0.17	2.67	∼0.03	∼0.53

Figure 1. Orbit of the MDS-1 satellite on February 11, 1st day of every month from March to July, and July 31 in 2002 in the X-Y plane in solar magnetospheric coordinates.

Figure 2. Location of the MDS-1 satellite in the L-MLT plane when the 68 auroral breakups were detected. Filled circles designate 17 events, in which local magnetic fiel dipolarization was observed. The magnetic fiel dipolarization was often detected around L=5.5-6.5, though some events can be seen even at $L<5$.

Figure 3. The magnetic fiel variation data (ΔV, ΔD, and ΔH) for 3 typical dipolarization events observed by MDS-1 in the deep inner magnetosphere (L=3.6-5.9). These events were found on (a) 19 March 2002 (Event 1), (b) 14 May 2002 (Event 2), and (c) 18 April 2002 (Event 3).

Figure 4. The Dst index for the dipolarization events observed on (a) 19 March 2002 (Event 1), (b) 14 May 2002 (Event 2), and (c) 18 April 2002 (Event 3). A dot in each panel indicates the onset time of dipolarization.

Figure 5. (a) Distribution of L values of the MDS-1 satellite for the 68 auroral breakups. (b) Distribution of L values of the MDS-1 satellite for the 17 selected dipolarization events. Gray shading indicates the number of dipolarization events occuring during storm growth phase. (c) Occurrence probability of dipolarization calculated from the number of dipolarizations (Figure 5b) divided by the number of auroral breakups (Figure 5a) in each L bin. Error bars represent 75% confidenc intervals that are calculated by using the maximum likelihood estimation. Occurrence probability for storm-related dipolarization is shown with gray shading.

Figure 6. Power spectra for 10-minute segments of ΔV and ΔH during/before the 3 events of magnetic fiel dipolarization, which are indicated with solid/dotted black curves, respectively. For easier identificatio of the change in spectral slopes around 3-5 sec in ΔV for all events and ΔH for Event 1 and 2, red dotted lines are fitte to power spectra in the long period portion (10-200 sec).

Figure 7. Example of the IMAGE/HENA images for Event 3. Top and bottom panels display ENA images of hydrogen in an energy range of 60-198 keV and oxygen in an energy range of 52-180 keV, respectively, at four different time intervals. Dipolarization began between the second and third images. In each image, the dipole magnetic fiel lines at 0000, 0600, 1200, and 1800 MLT are drawn for L value of 4 and 8. A "backward C-shaped" area outlined in red in the top-leftmost panel indicates the area over which ENA flu was integrated, to examine the temporal variations in ENA flu in detail.

Figure 8. Temporal variations of ENA flu for the 3 dipolarization events integrated over the nightside ring current region (the "backward C-shaped" region in Figure 7) and normalized as measured at a radial distance of 8 R_E. From top to bottom, data are for (a) the 19 March 2002 event (Event 1), (b) the 14 May 2002 event (Event 2), and (c) the 18 April 2002 event (Event 3). Red and blue lines indicate hydrogen and oxygen ENA flu es, respectively.

Figure 9. Schematic figure of scenarios to explain the significan increase of the O^+ ion contribution to the ring current during magnetic storms. Scenarios I through III are those proposed by previous studies: (I) direct transport of O^+ ions from the ionosphere to the ring current and acceleration on their way, (II) transport of O^+ ions from the ionosphere to the near-Earth plasma sheet through the lobe followed by adiabatic transport into the ring current and betatron acceleration, and (III) transport of O^+ ions from the ionosphere to the near-Earth plasma sheet through the lobe followed by nonadiabatic transport and acceleration by an inductive electric fiel due to dipolarization. Scenario IV is a new one suggested by the present observations. Thermal O^+ ions exist in the outer plasmasphere at L=2.0-5.0 (i.e., the oxygen torus) before storms, and they are locally and nonadiabatically accelerated by fluctuation associated with dipolarization in the ring current region.

Figure 1

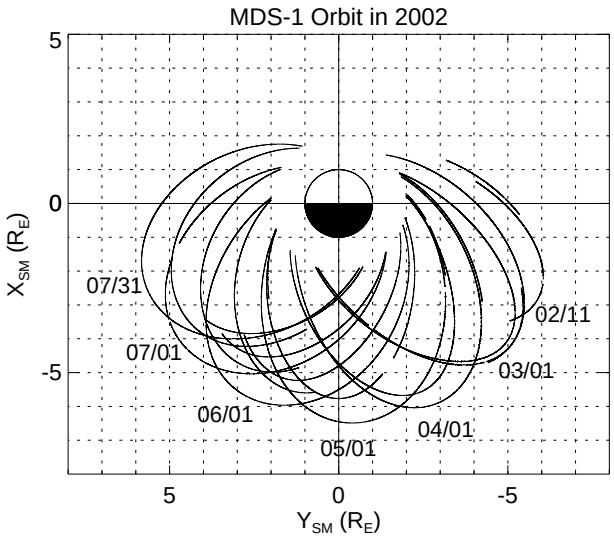

Figure 2

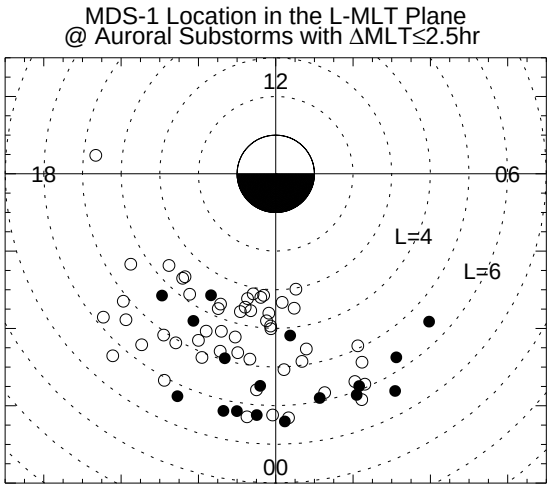

Figure 3

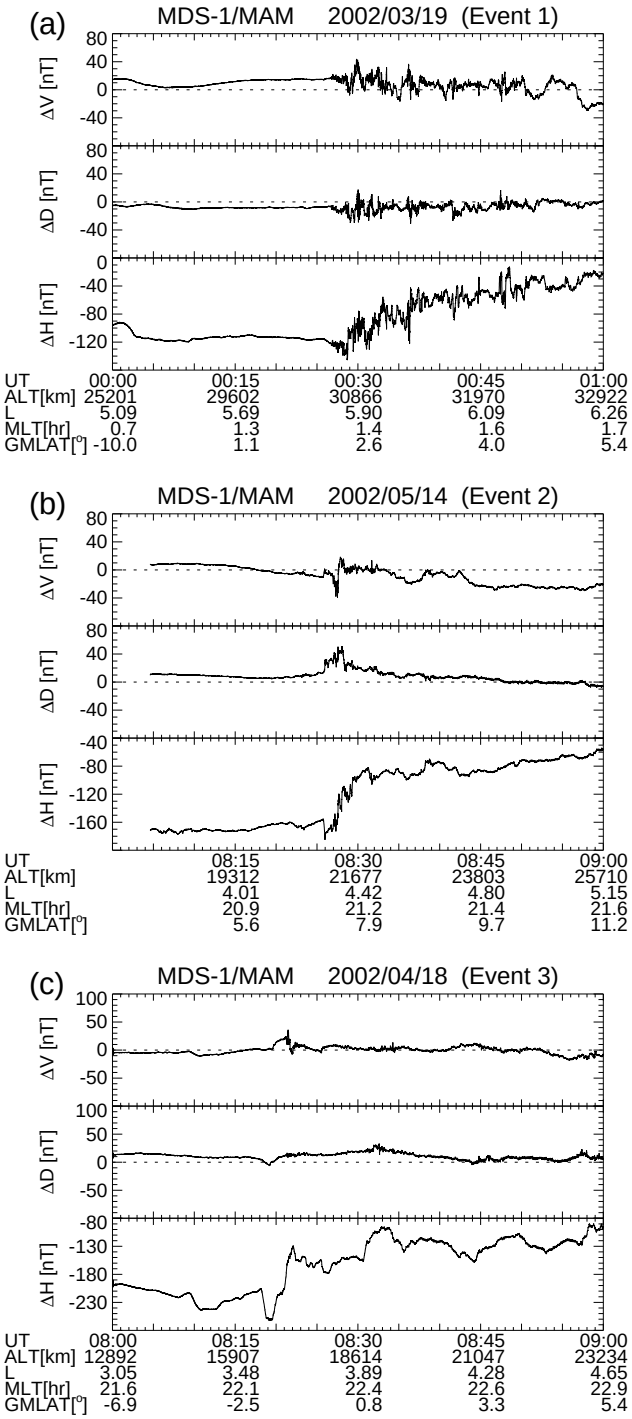

Figure 4

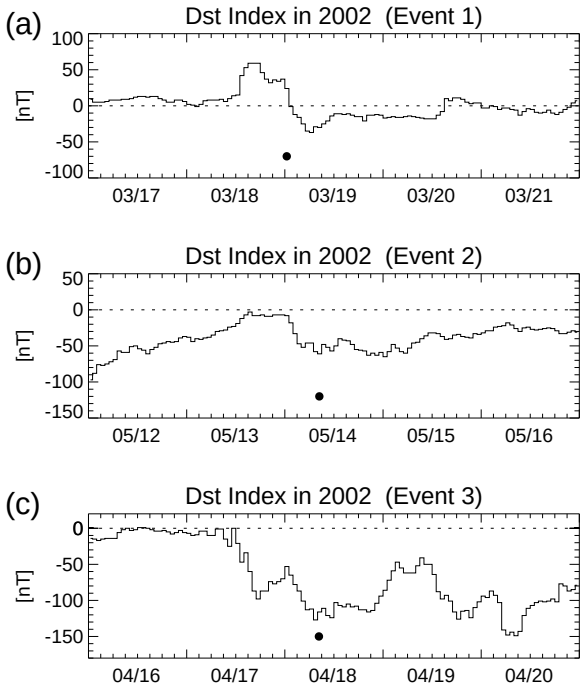

Figure 5

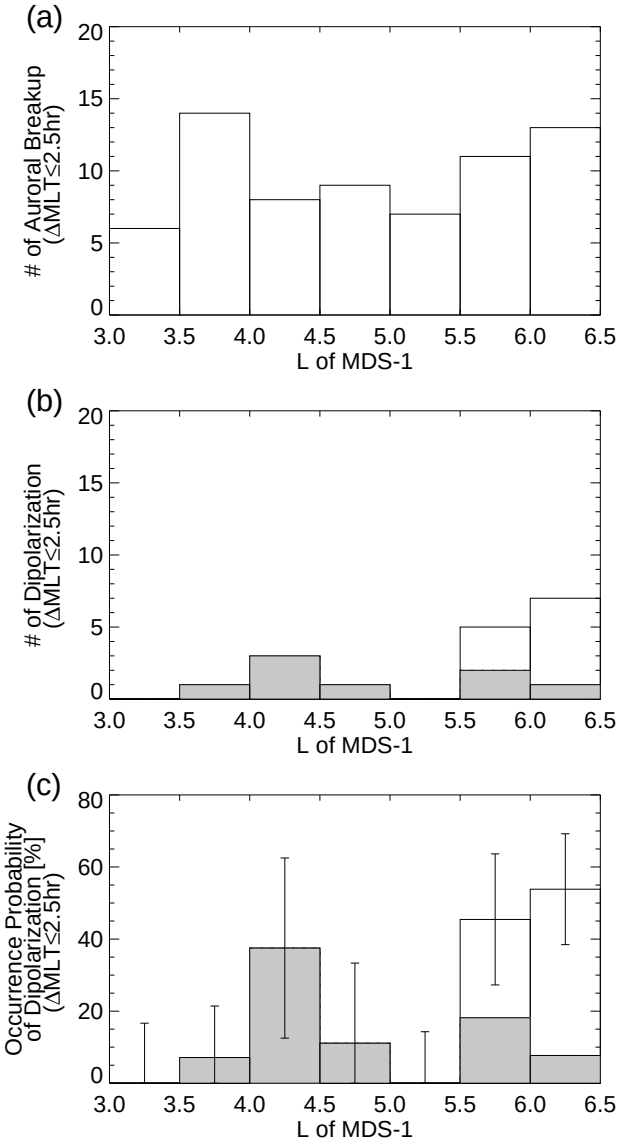

Figure 6

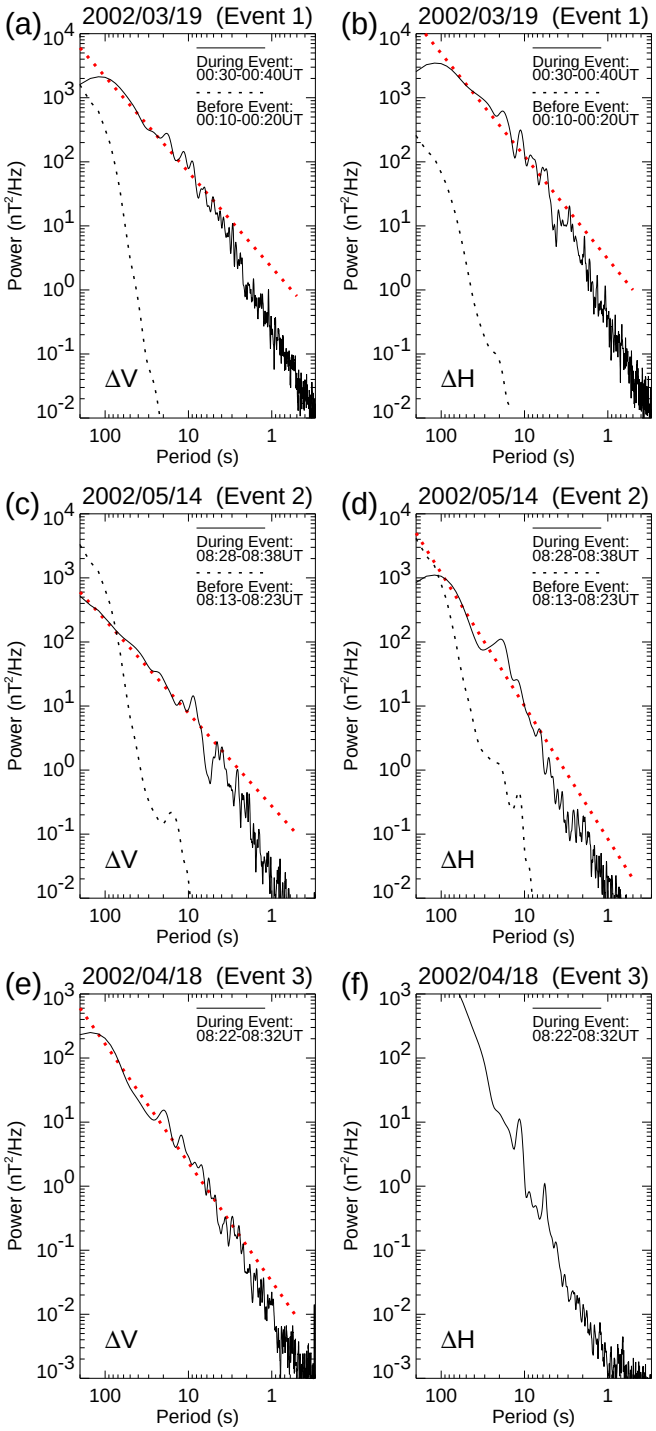

Figure 7

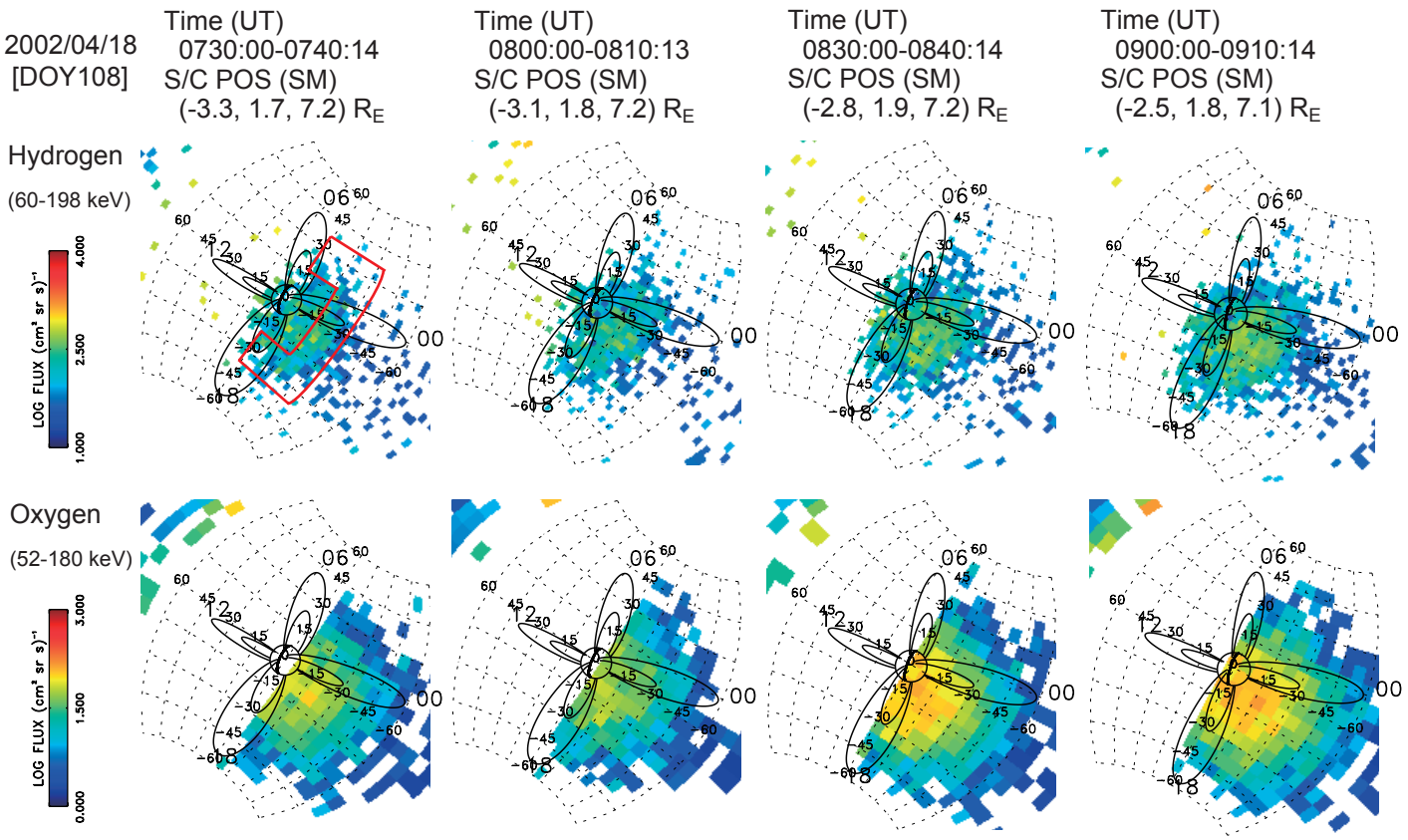

Figure 8

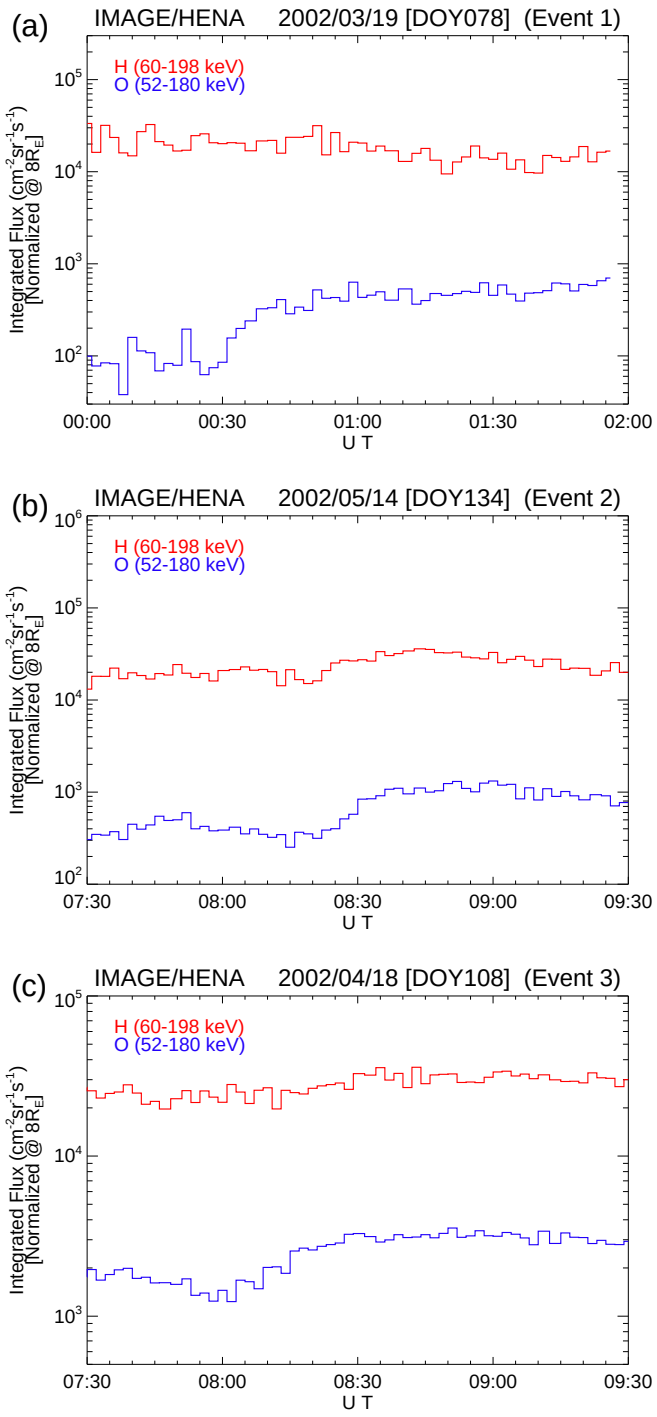

Figure 9